Supplement

Alternative sample names:

H1	H2	W1	W2	W3	W4	D1	D2	V
BA-3	BA-4	AA-5	BA-1	BA-2	BA-5	AA-2	AA-3	V3-5

S1 Figures

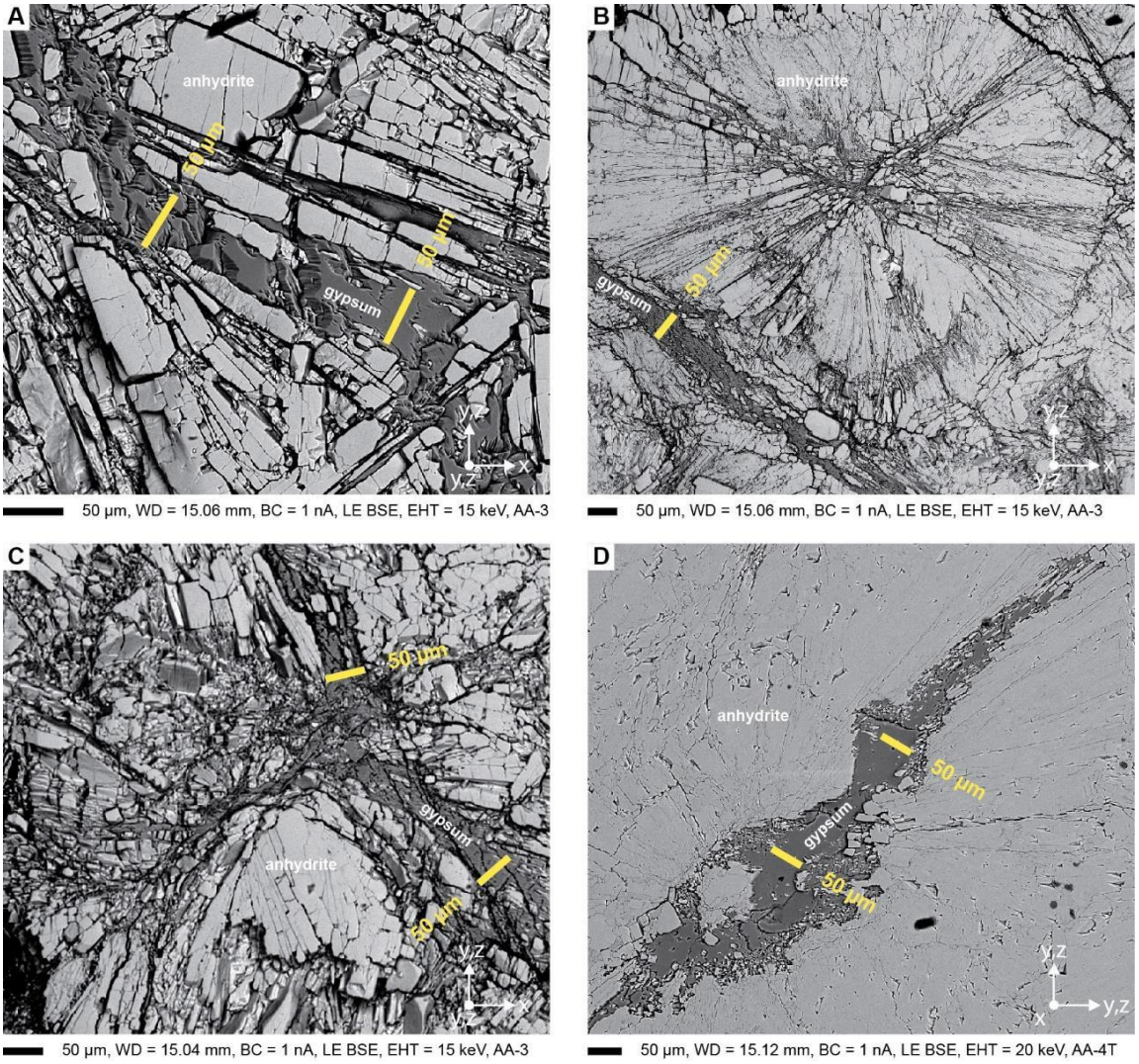

Fig. S1: Electron backscatter images of Òdena anhydrite. A: gypsum vein in anhydrite, sample D2. B: Gypsum vein next to a spherulite with gypsum in the center and between grains, sample D2. C: Gypsum vein in anhydrite, sample D2. D: Gypsum vein cutting through spherulites, sample not used for experiments.

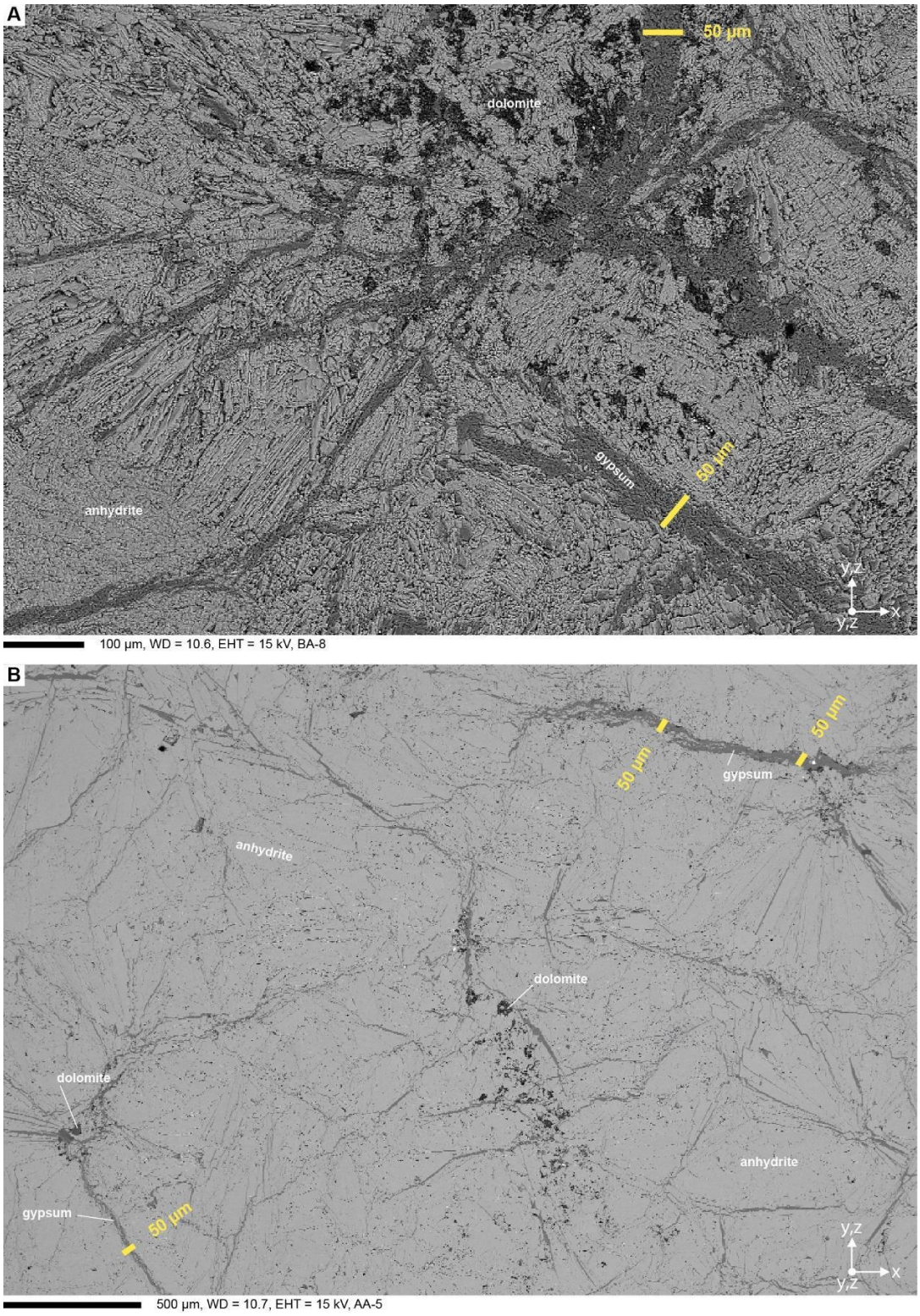

Fig. S2: Electron backscatter maps of Òdena anhydrite. A: Gypsum vein systems, sample not used for experiments. B: Map of sample W1.

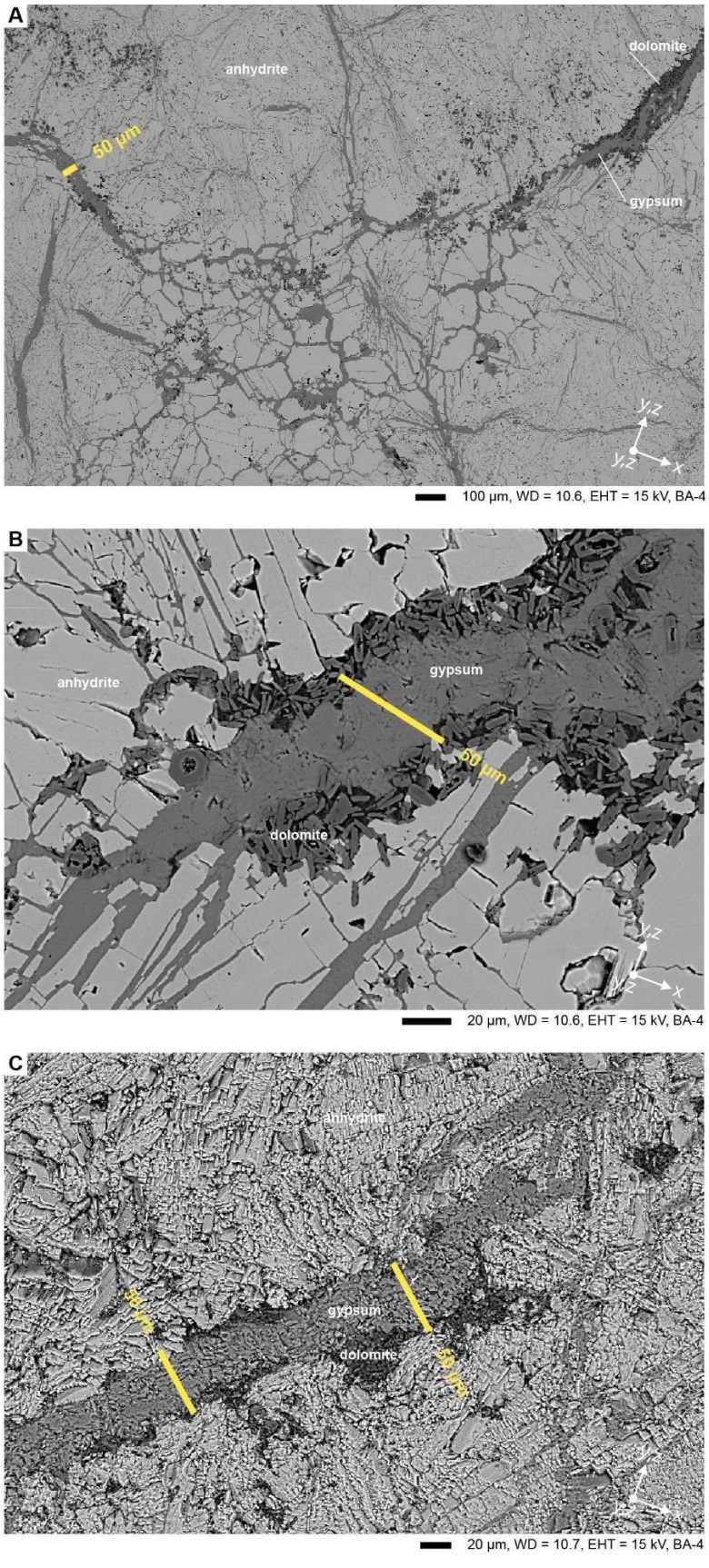

Fig. S3: Electron backscatter images of Òdena anhydrite sample H2.

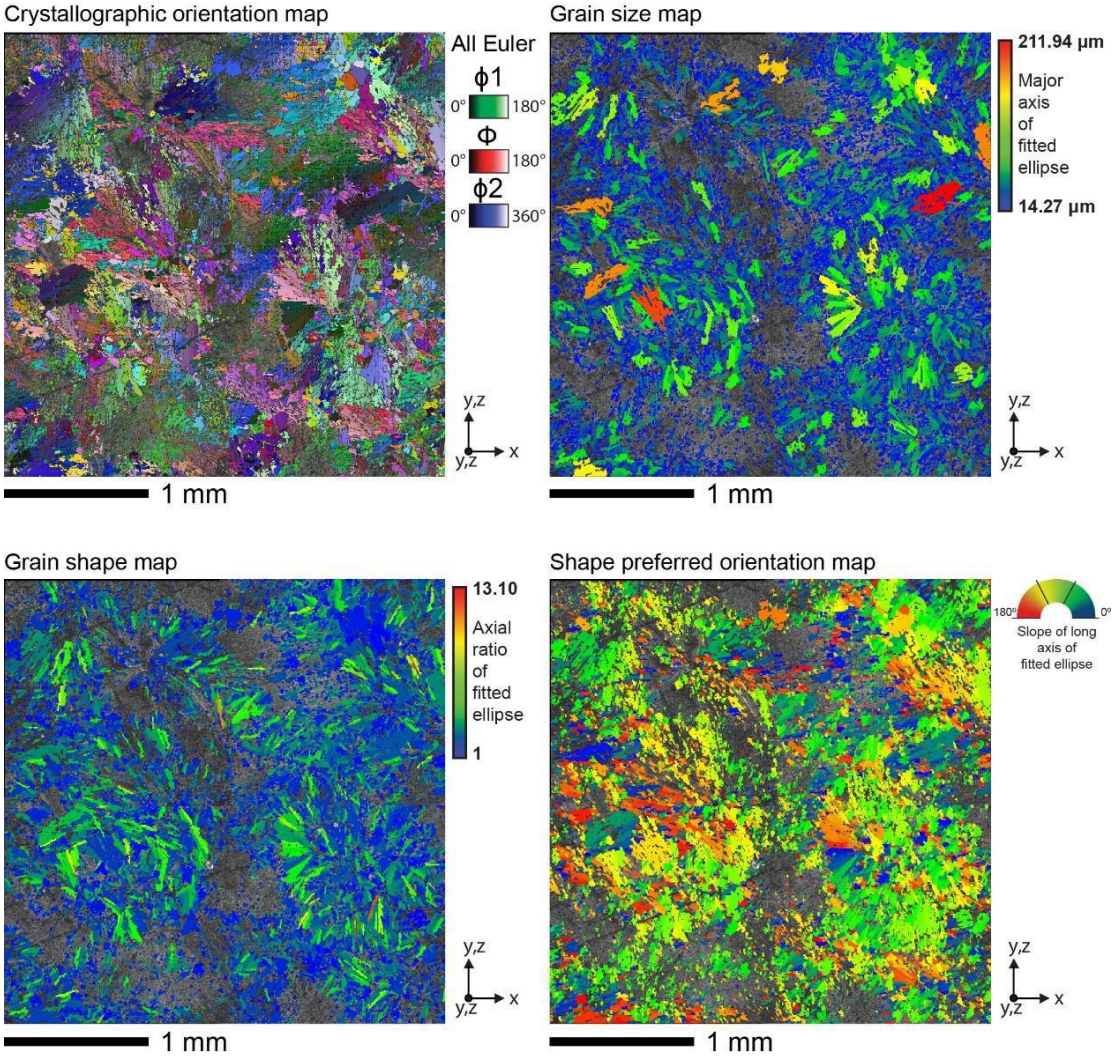

Fig. S4: Electron backscatter diffraction analysis of initial Òdena anhydrite sample material. See Figure 2c,d for IPFx EBSD map and equal area, lower hemisphere pole figures of anhydrite. Step size was 4 µm.

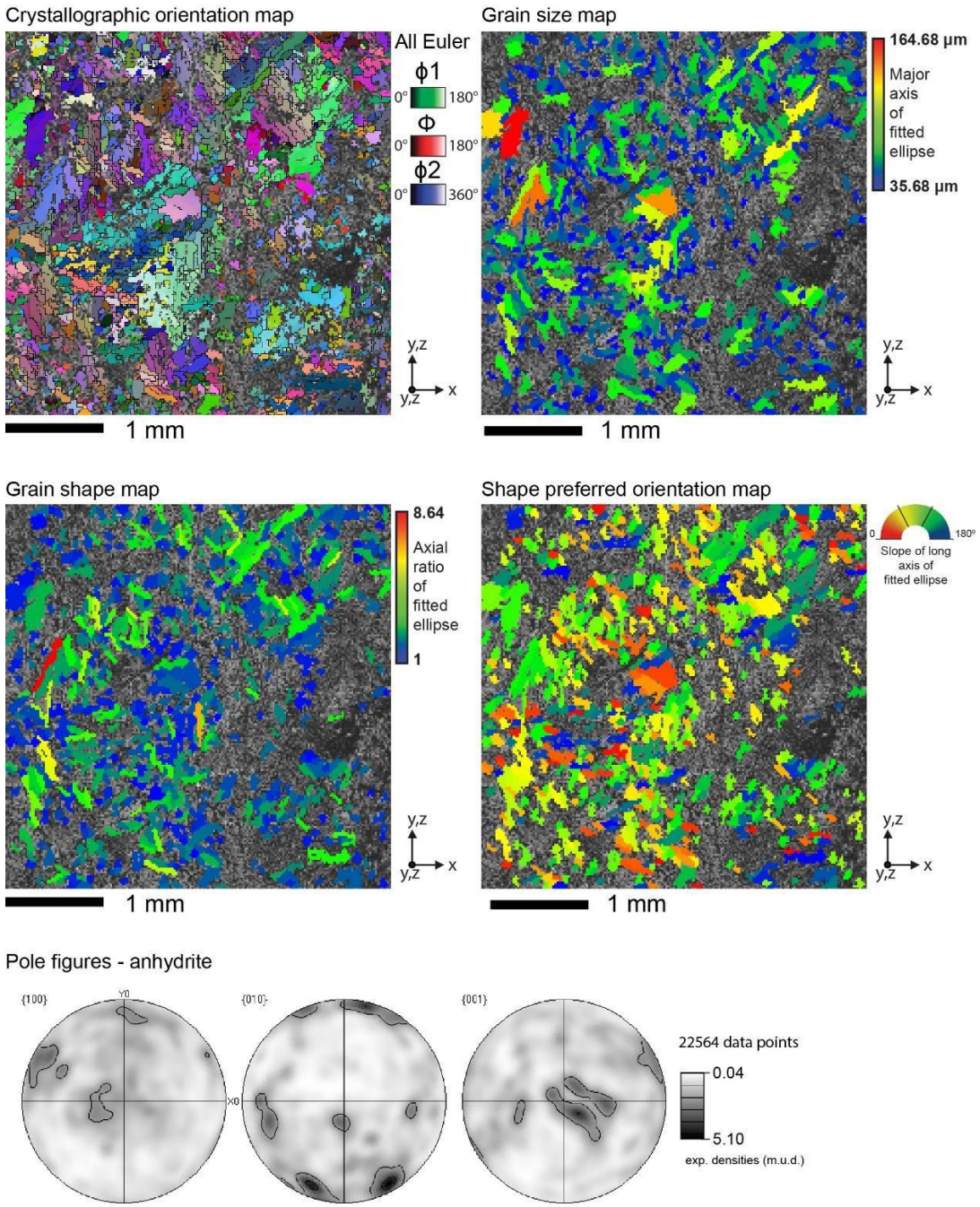

Fig. S5: Electron backscatter diffraction analysis of initial Òdena anhydrite sample material, including equal area, lower hemisphere pole figures of anhydrite. Step size was 10 µm.

H1 (BA-3, CSDC)

W1 (AA-5, ‘wet’)

W2 (BA-1, ‘wet’)

W3 (BA-2, ‘wet’)

D1 (AA-2, dry)

V (V3-5, dry)

Fig. S6: Photographs of post-experiment cores after undergoing all three test modes.

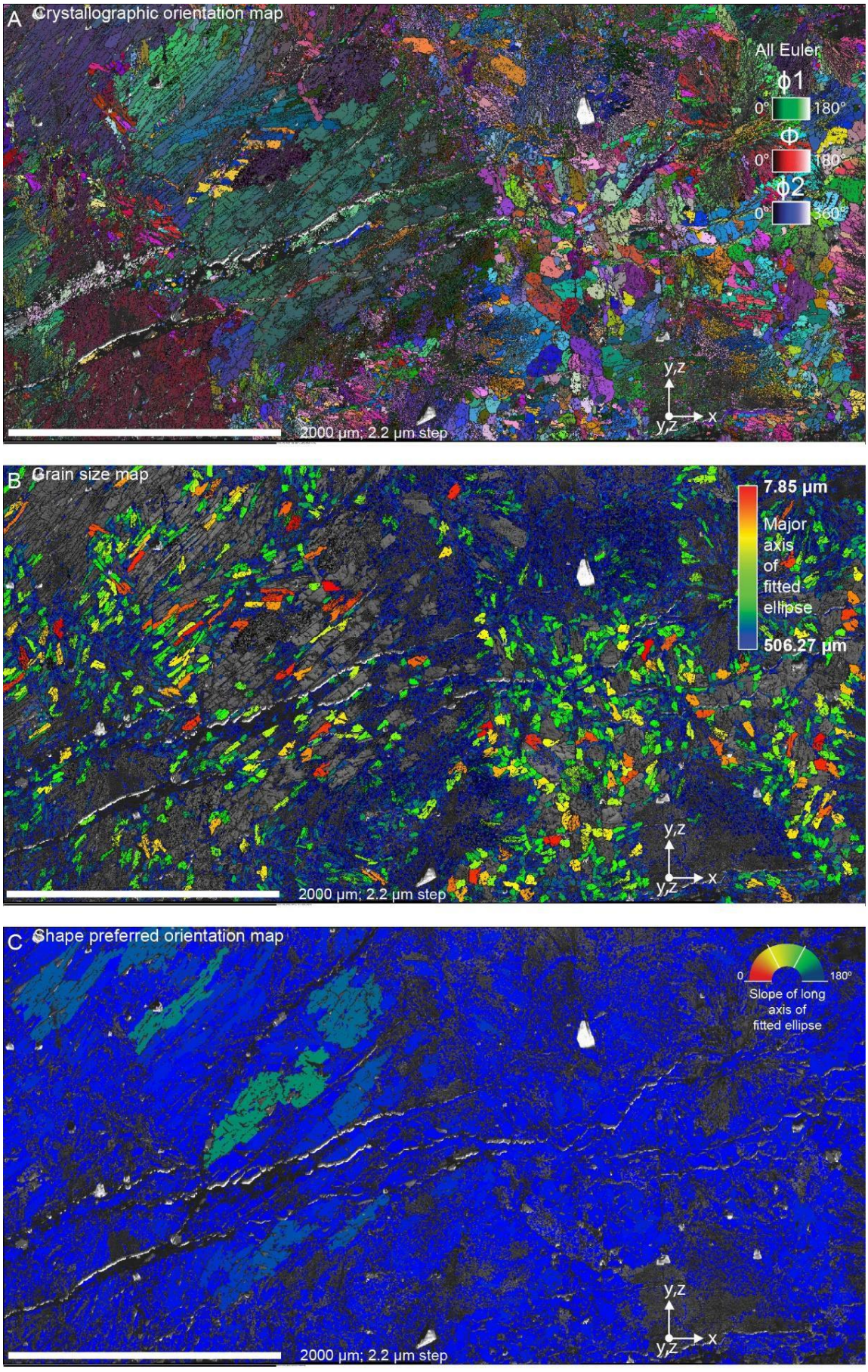

$\sigma_1 \rightarrow \quad \leftarrow \sigma_1$

Fig. S7: Additional electron backscatter diffraction analysis from the area of sample W1 ('wet' mode experiment).

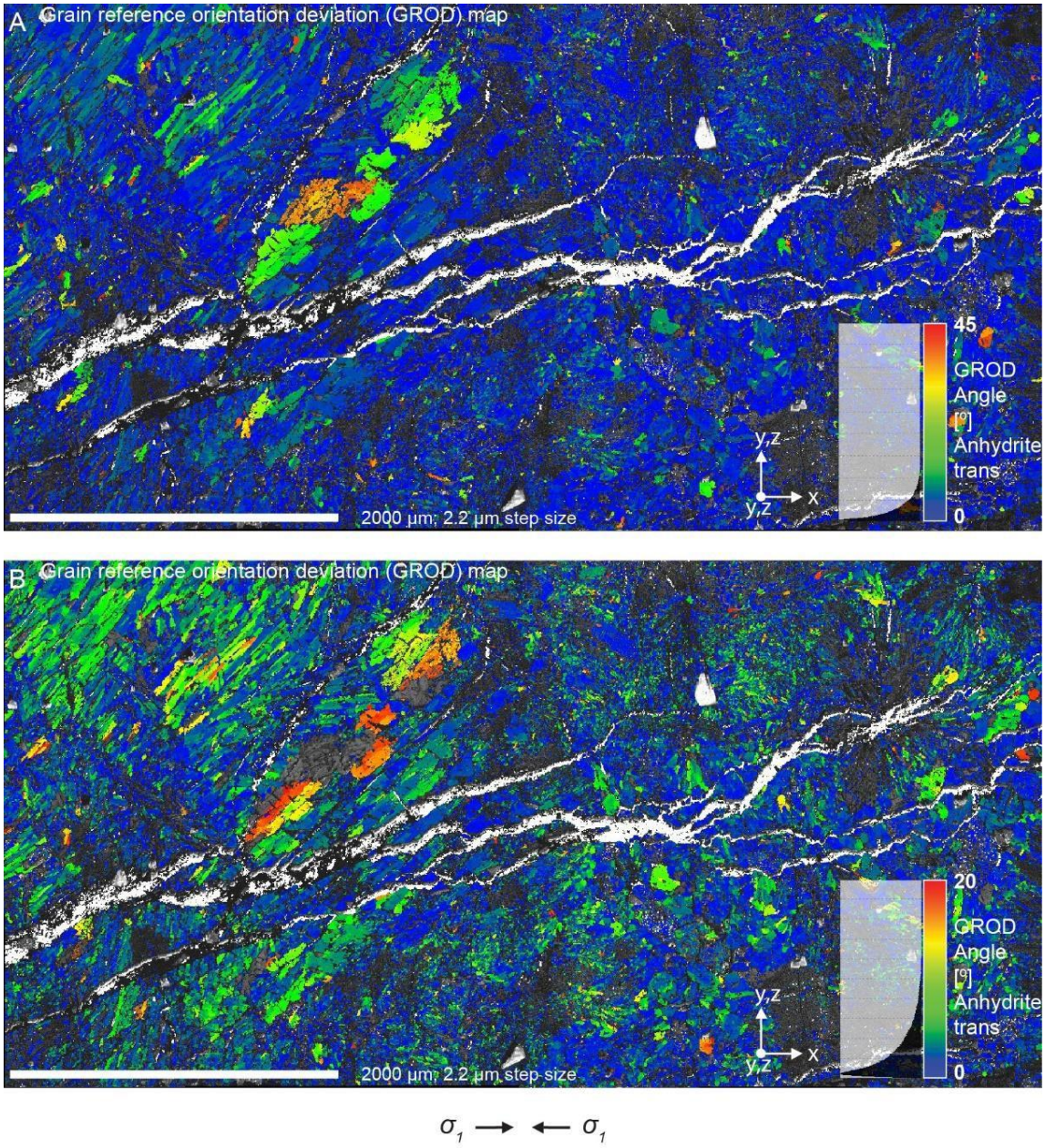

Fig. S8: Grain reference orientation deviation (GROD) maps of anhydrite from the Area 1 electron backscatter diffraction dataset of W1 ('wet' mode experiment). GROD analysis shows orientation heterogeneities that form during deformation, and hence displays internal deformation of grains. Each pixel is coloured based on the misorientation of the point relative to a reference orientation for the grain to which the point belongs to. Component limits (GROD angle) were at a range of 0 to 45° for A and to 0 to 20° for B. Exclusion of higher angles results in loss of data and is more sensitive to low angle heterogeneities.

GROD analysis shows that the blocky area has slightly higher internal deformation, with angles ~40° in one large grain and ~20° in surrounding grains. The rest of the anhydrite appears heterogeneous, with GROD angles commonly between 0 and 15°.

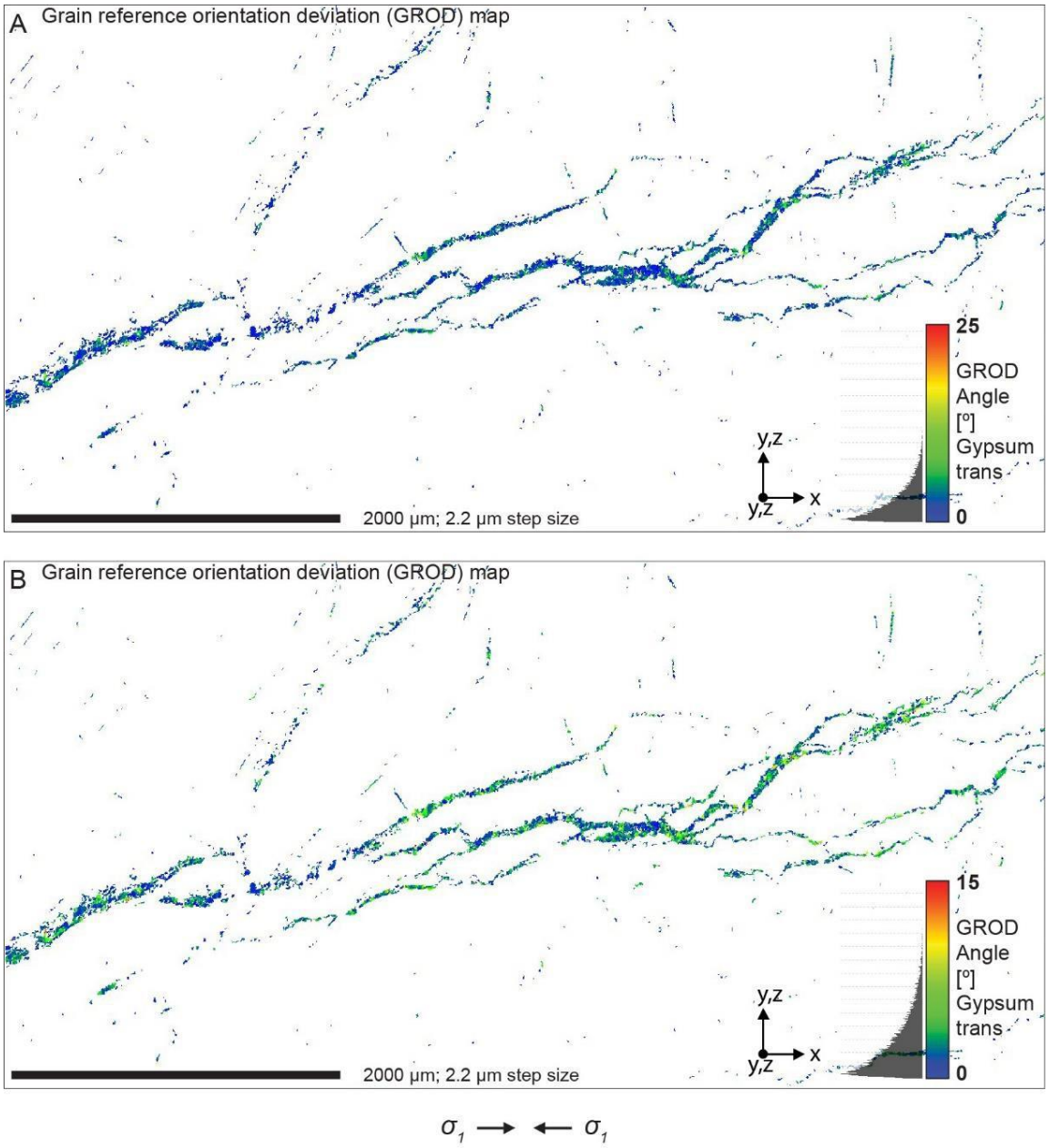

Fig. S9: Grain reference orientation deviation (GROD) maps of vein-hosted gypsum from the Area 1 electron backscatter diffraction dataset of W1 (post 'wet' mode experiment). Component limits (GROD angle) were at a range of 0 to 25° for A and to 0 to 15° for B. Exclusion of higher angles results in loss of data and is more sensitive to low angle heterogeneities.

Summary grain statistics

			no grains	Grains%	Area	%	AVG d	STDV d	AVG slope	STDV slop	AVG AR	STDV AR
anh	2	23453	23452	90.76905	1.03E+07	9.508E+01	16.86657	16.54946	84.1283	51.02407	2.082103	0.896492
gyp	23454	25838	2385	9.230948	5.33E+05	4.923E+00	14.70951	8.242795	74.57741	49.84299	2.15751	1.020427
total			25837		1.08E+07							
EX	16.62	Average, expectation										
D^2X	249.65	Variance, dispersion										
s	15.8	Standard deviation										
s/EX	0.95066	Coefficient of variation										
Xmin	7.8501	Minimum value										
Xmax	506.27	Maximum value										
N	25760	Size of the data set										

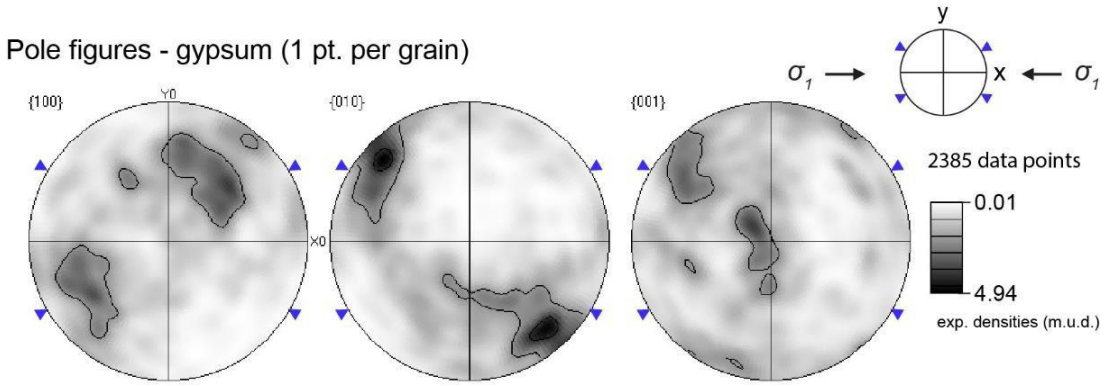

Fig. S10: Grain statistical data and one point per grain, equal area, lower hemisphere pole figures of gypsum from analysis of the electron backscatter diffraction data set of Area 1 in sample W1 (post 'wet' mode experiment).

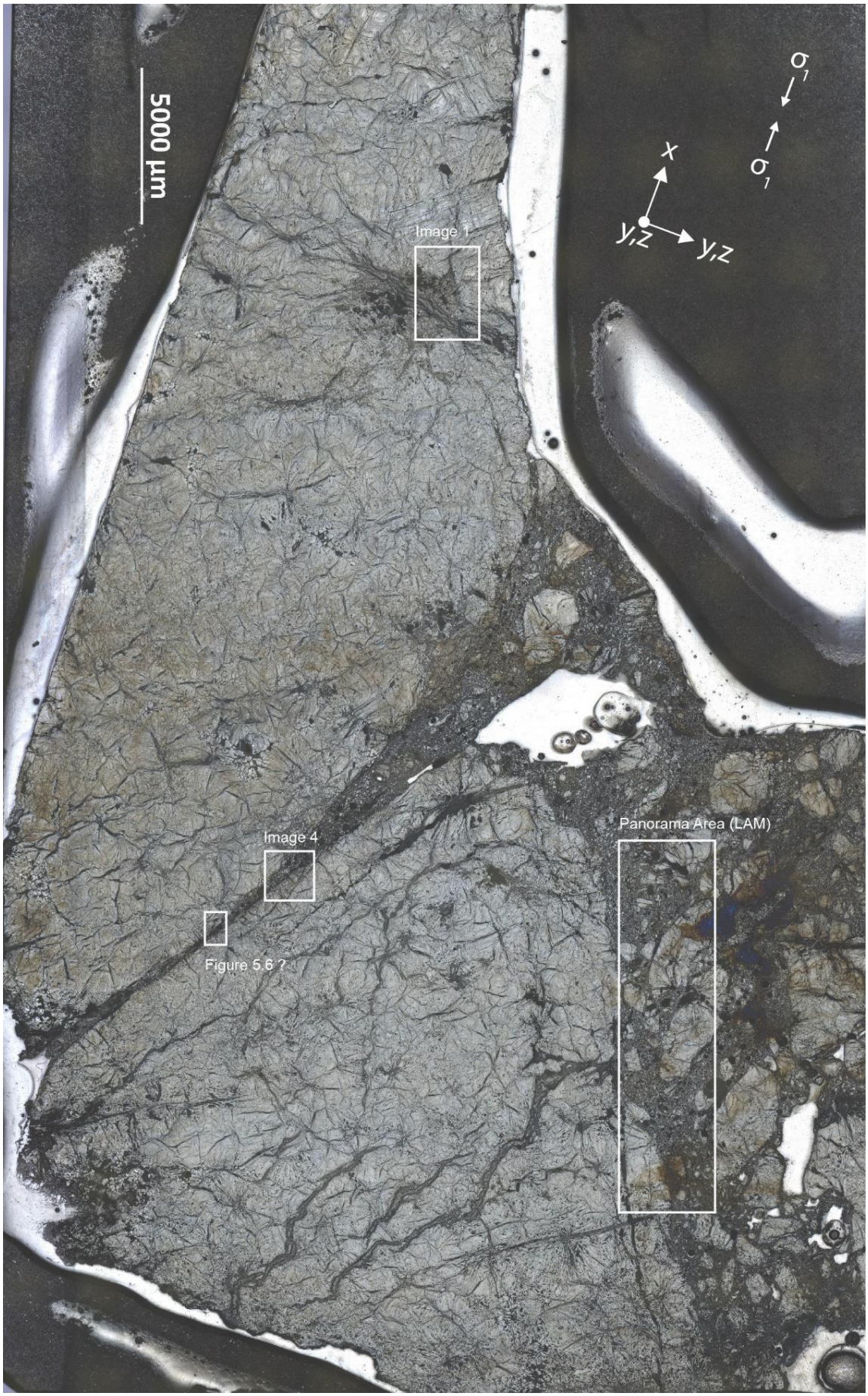

Fig. S11: Reflected light microscopy images of a thin section of sample H2 (post CSDC mode experiment) with areas marked where further analysis was done. The area marked as Figure 5.6? is an estimate, as the thin section was polished for EBSD between imaging.

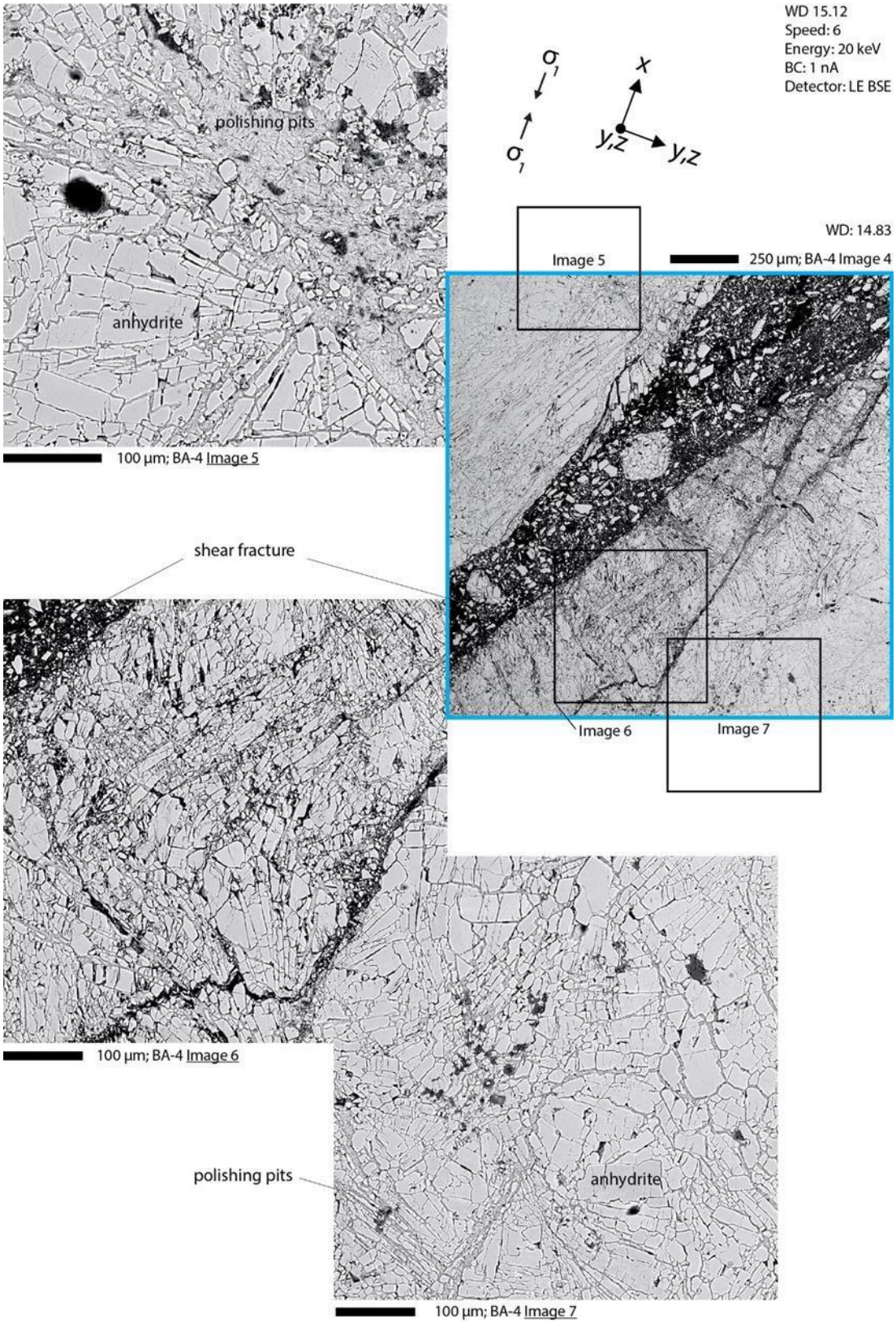

Fig. S12: Backscatter electron images of H2 after CSDC. Image 4: shear fracture map, location marked in Fig. S11. Image 5: ~ 100 µm wide polishing pit (gypsum vein that lost gypsum due to polishing), and spherulitic radial anhydrite laths. Image 6: cataclastic zone with shear bands between the open shear fracture (no matrix, filled with clasts). A long fracture divides the cataclastic zone (Image 6) from the intact fabric of Image 7.

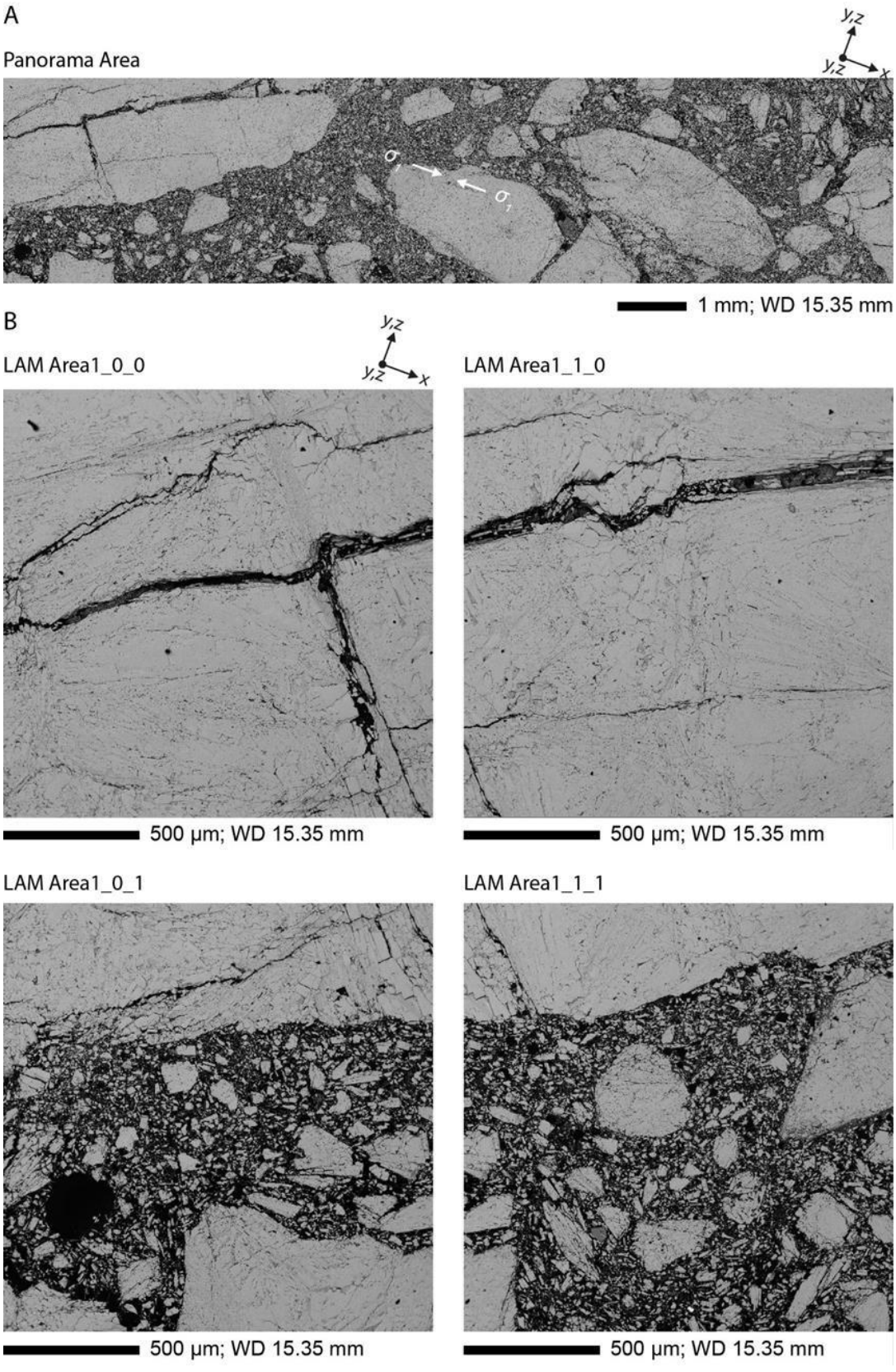
A
Panorama Area
y,z
y,z
x
σ1
σ1
1 mm; WD 15.35 mm
B
LAM Area1_0_0
y,z
y,z
x
LAM Area1_1_0
500 µm; WD 15.35 mm
500 µm; WD 15.35 mm
LAM Area1_0_1
LAM Area1_1_1
500 µm; WD 15.35 mm
500 µm; WD 15.35 mm

C

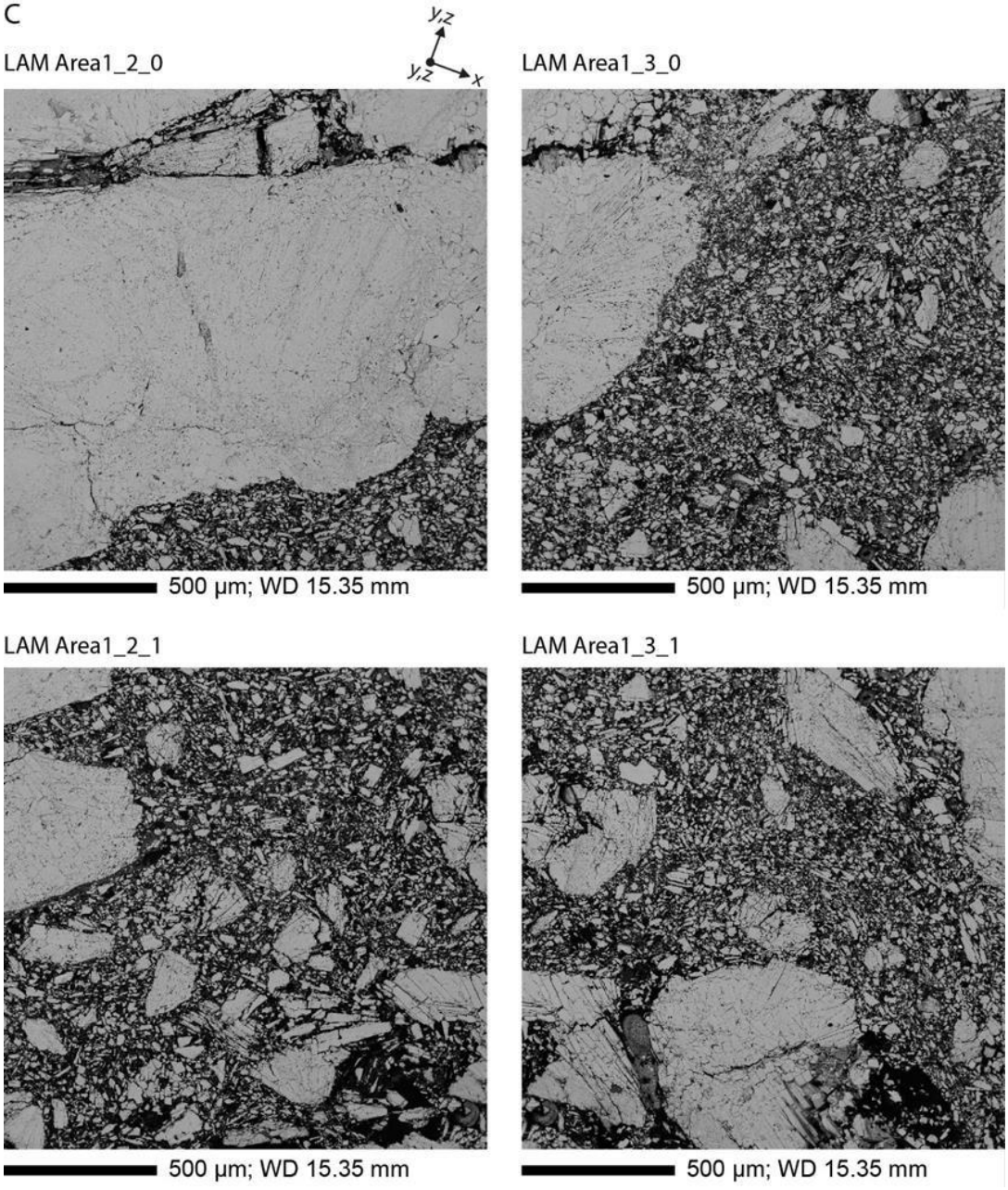
LAM Area1_2_0
y,z
y,z
x
LAM Area1_3_0
500 µm; WD 15.35 mm
500 µm; WD 15.35 mm
LAM Area1_2_1
LAM Area1_3_1
500 µm; WD 15.35 mm
500 µm; WD 15.35 mm

D

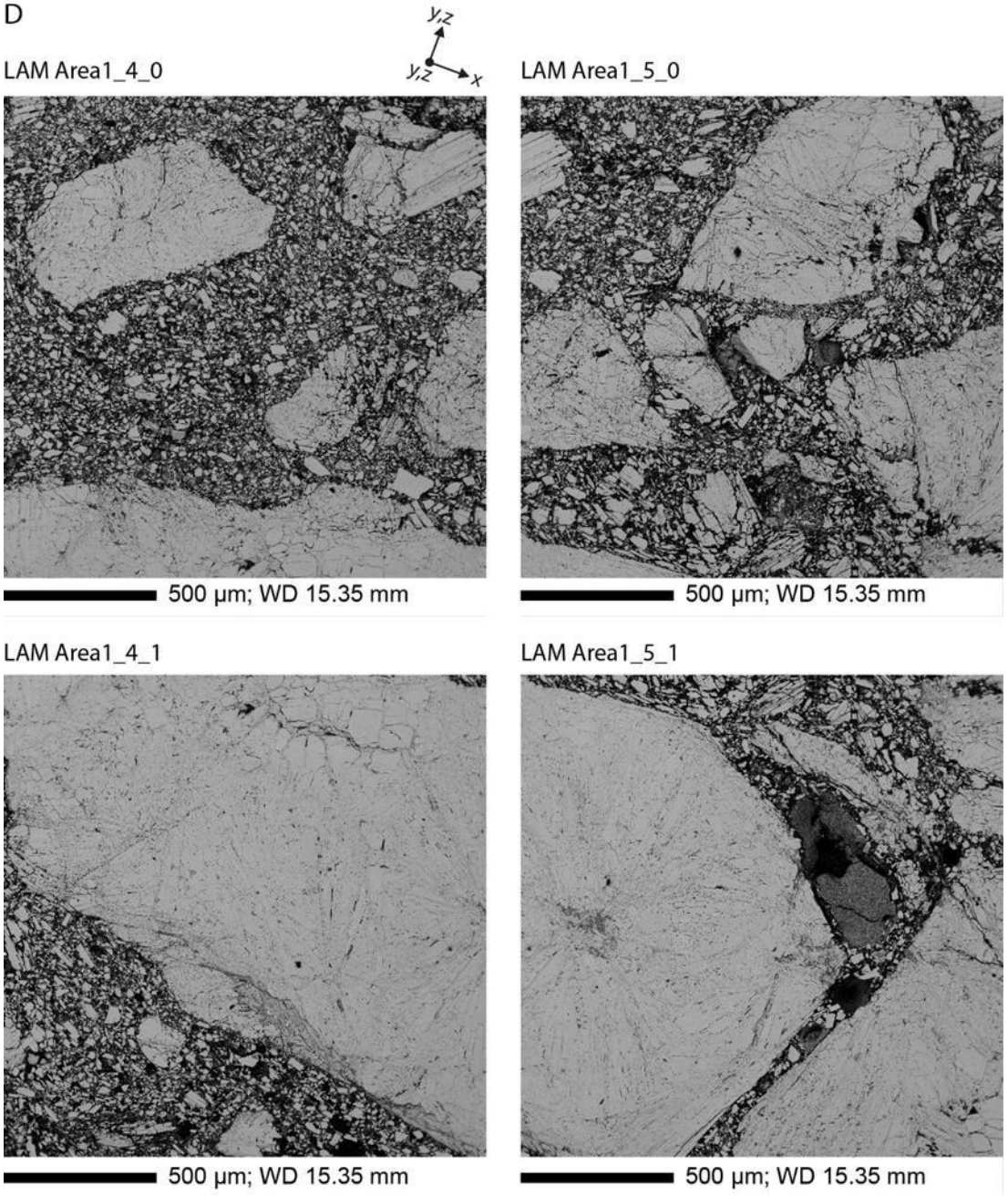
y,z
y,z
x
LAM Area1_4_0
LAM Area1_5_0
500 µm; WD 15.35 mm
500 µm; WD 15.35 mm
LAM Area1_4_1
LAM Area1_5_1
500 µm; WD 15.35 mm
500 µm; WD 15.35 mm

E

LAM Area1_6_0

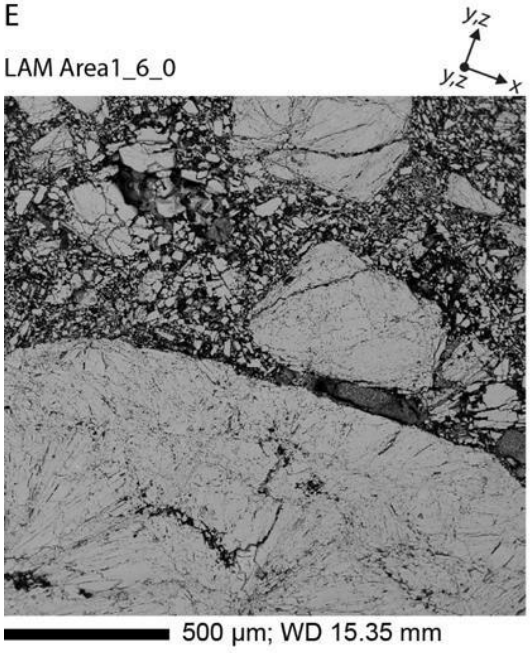

LAM Area1_7_0

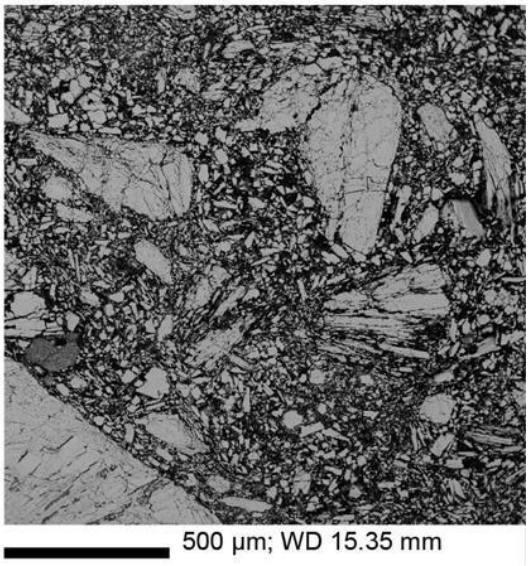

LAM Area1_6_1

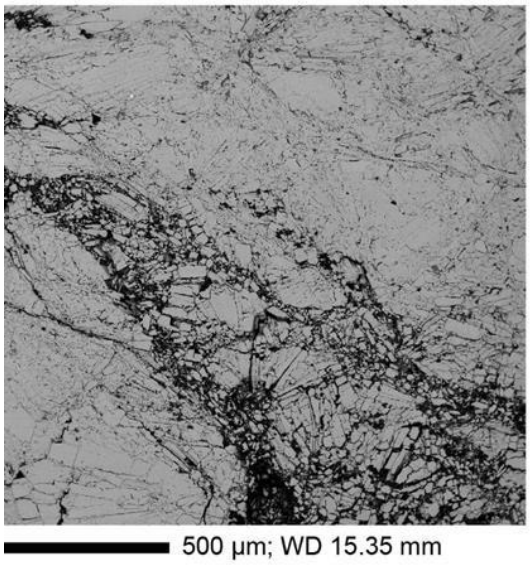

LAM Area1_7_1

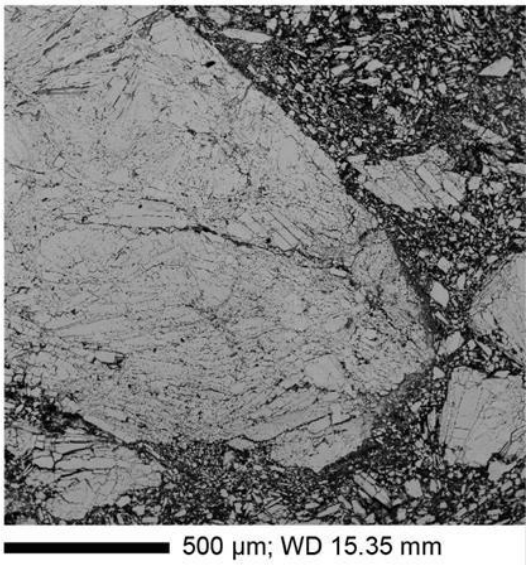

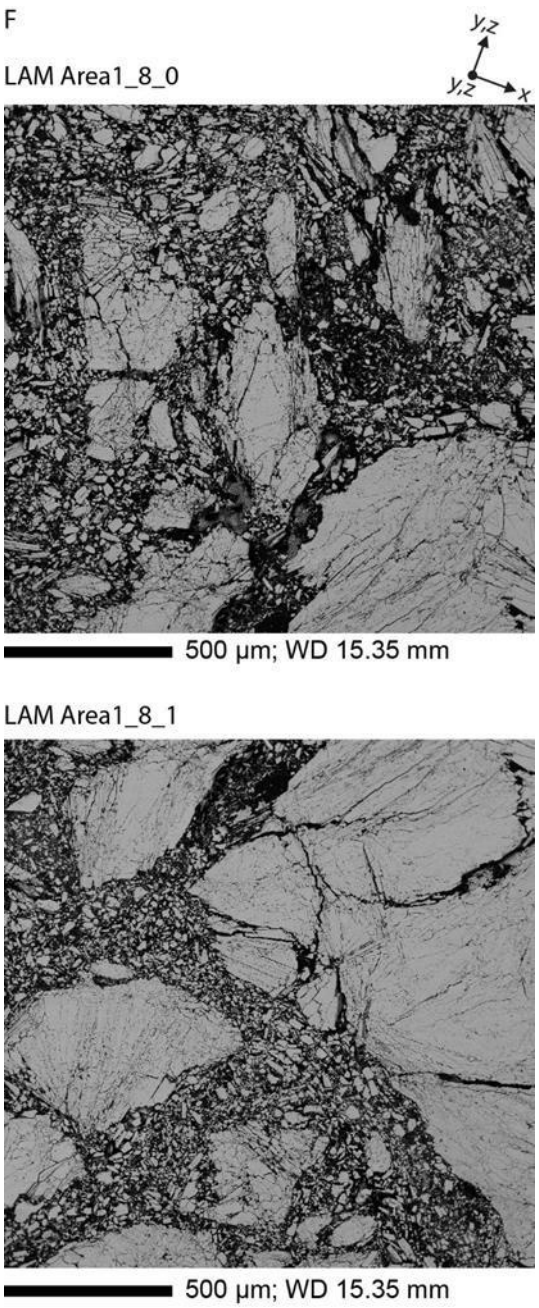

Fig. S13: Backscatter electron panorama of a cataclastic shear zone in H2 after constant stress differential compaction. A: Panorama, B to F single panorama frames. Light grey: anhydrite, medium grey: gypsum, black: open fractures. A mixed matrix of < 100 µm sized gypsum and anhydrite particles contains up to millimetre-scale anhydrite clasts with intense internal fracturing and low gypsum content. The amount of gypsum is difficult to identify from the images, as the sample lost gypsum due to polishing. The location of the panorama is marked as Panorama Area (LAM) in Fig. S11.

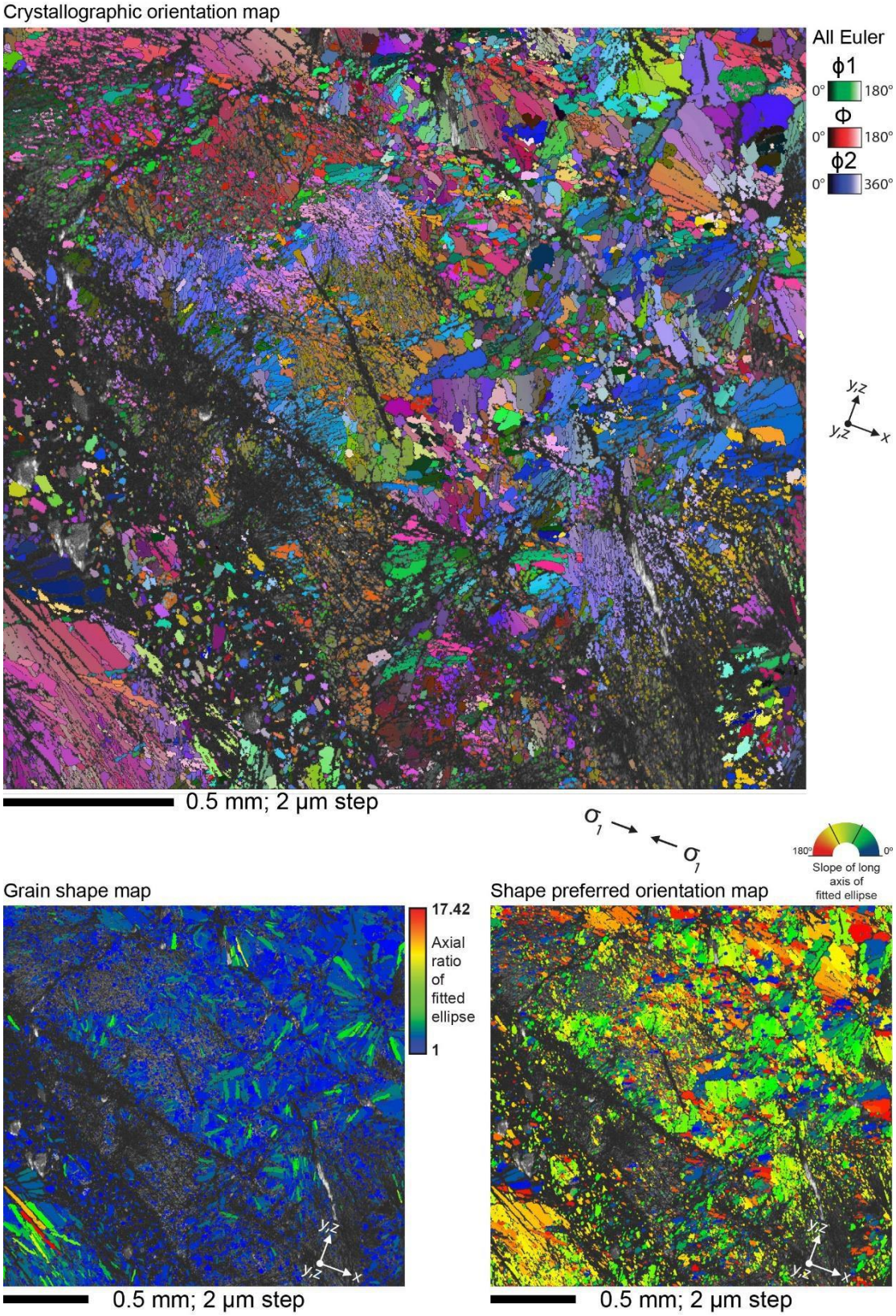

Fig. S14: Electron backscatter diffraction analysis of a cataclastic shear zone and surrounding fabric with spherulites in sample H2 after constant stress differential compaction (CSDC). Gypsum was not detected, due to polishing pits.

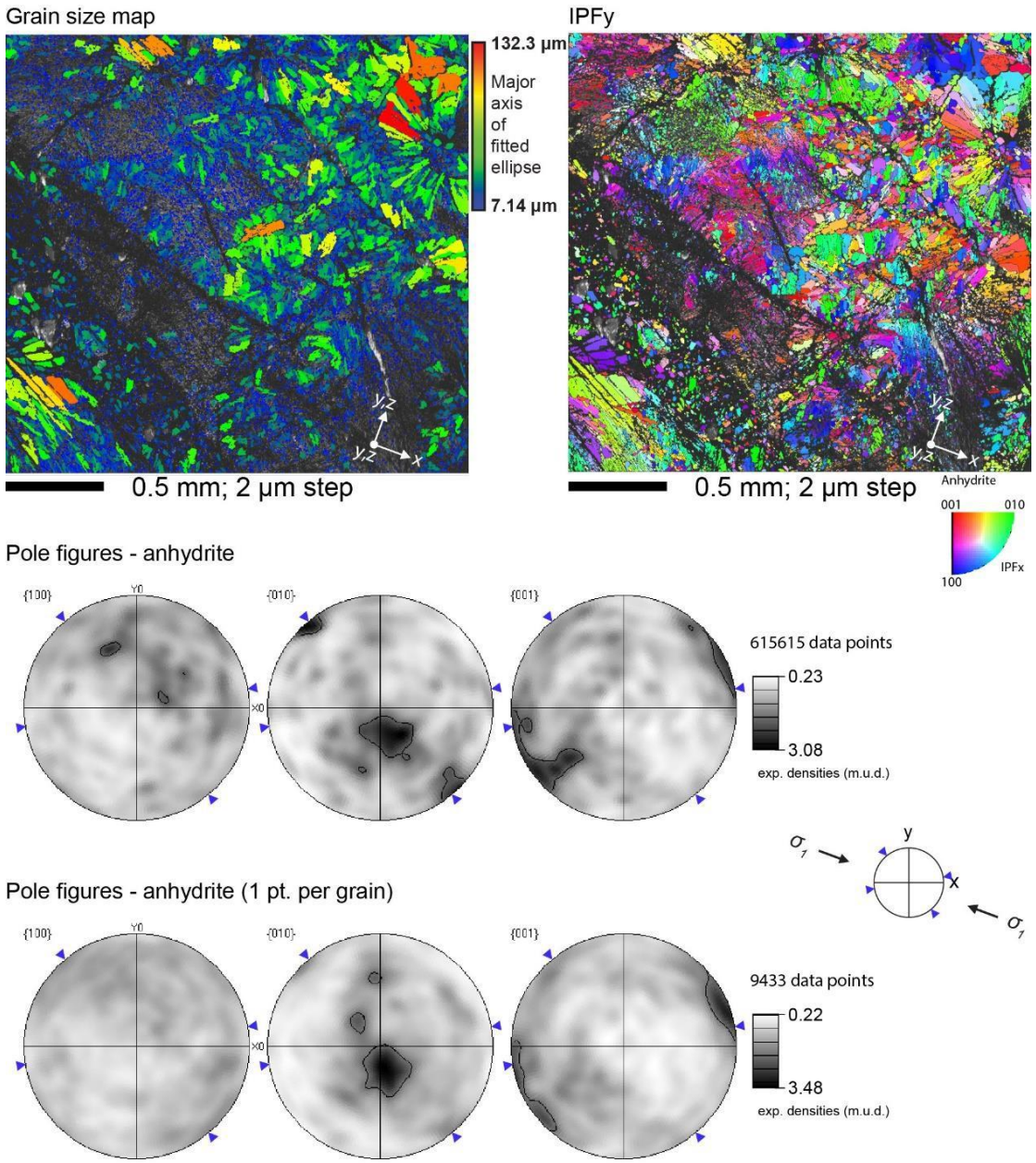

Fig. S15: Second part of backscatter diffraction analysis of a cataclastic shear zone in sample H2. Equal area, lower hemisphere pole figures of anhydrite based on the complete dataset and based on 1 point per grain subset.

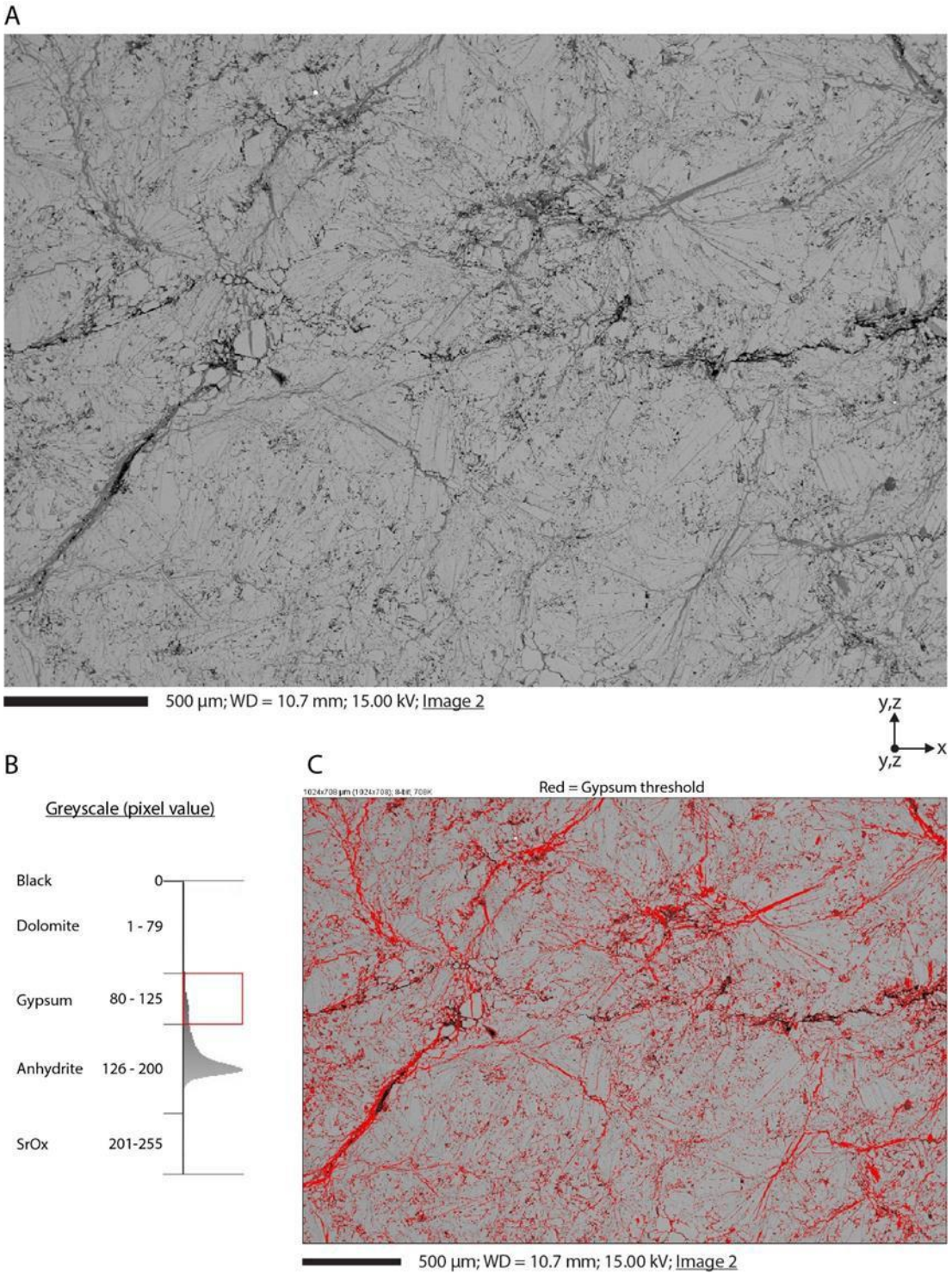

Fig. S16: Phase content analysis via greyscale threshold (ImageJ) from A: backscatter electron Image 2 of Òdena quarry sample D2 (AA-3). This sample went through a dry mode test and no signs of new formed gypsum was found. B: Greyscale threshold settings defined to quantify %. SrOx = accessory phases. C: Image 2 with all pixels that fall into the gypsum threshold in red. See Table S1 for further results.

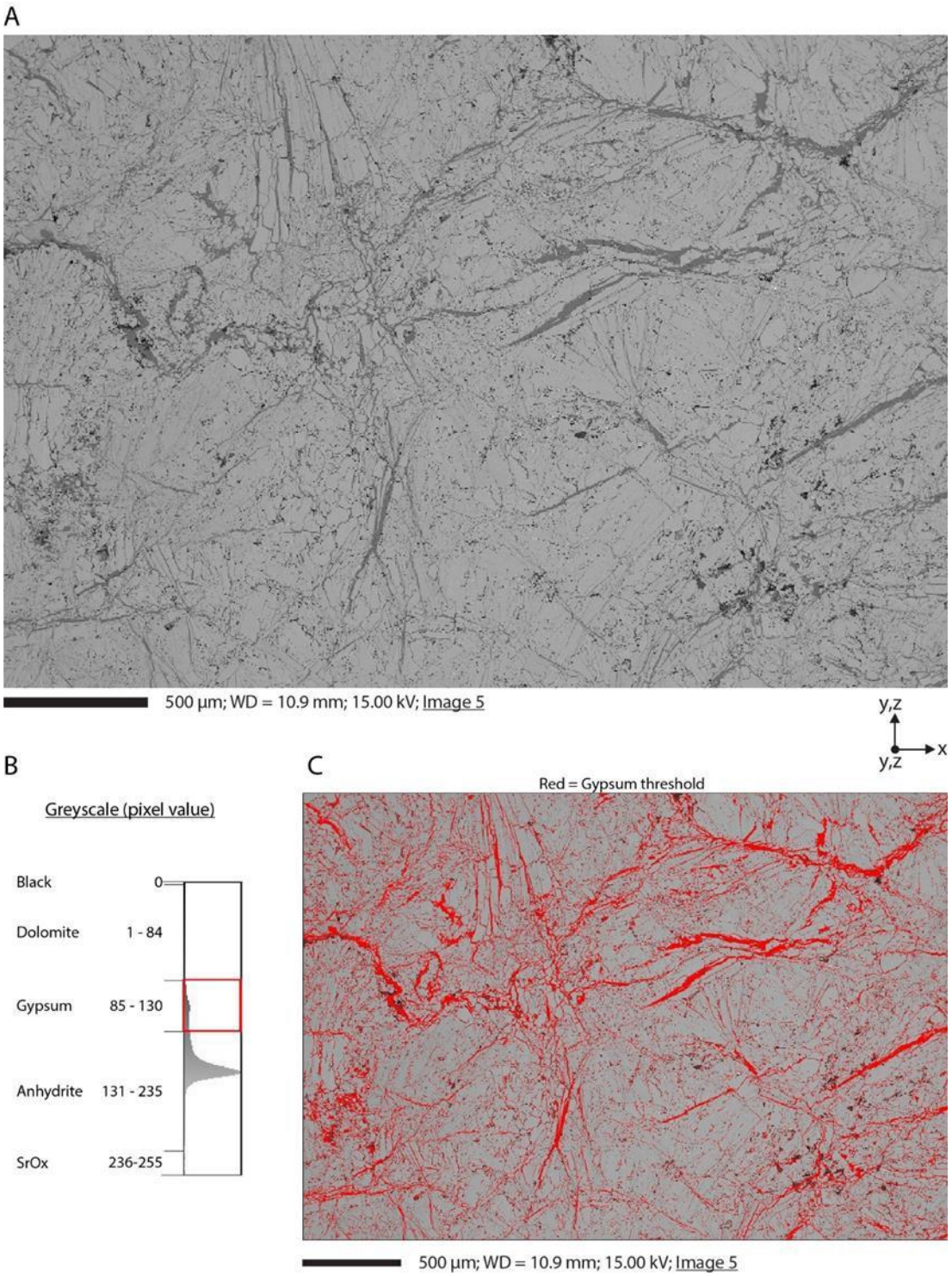

Fig. S17: Phase content analysis via greyscale threshold (ImageJ) from A: backscatter electron Image 5 of Òdena quarry sample D2 (AA-3). B: Greyscale threshold settings defined to quantify %. SrOx = accessory phases. C: Image 5 with all pixels that fall into the gypsum threshold in red. See Table S1 for further results.

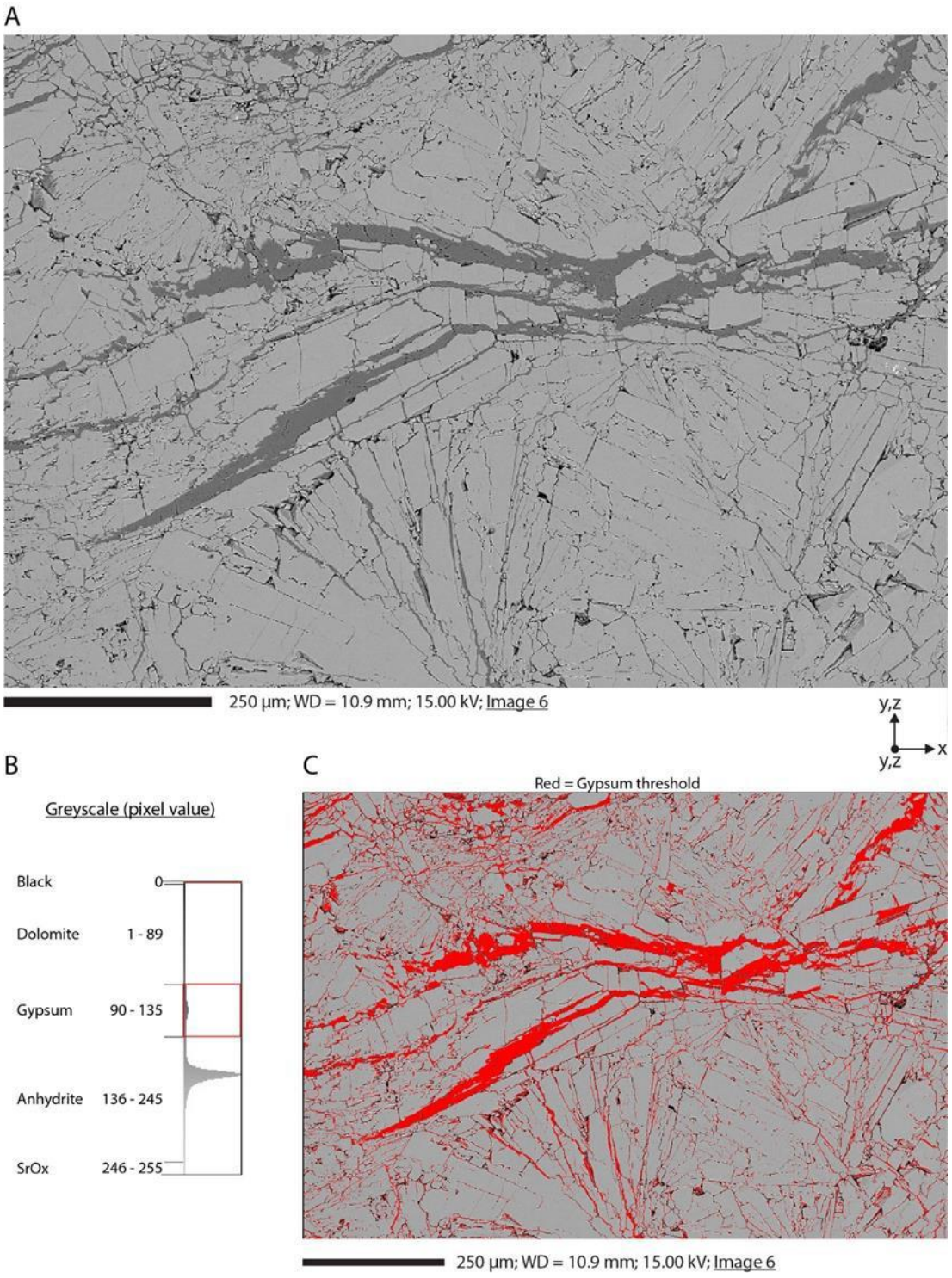

Fig. S18: Phase content analysis via greyscale threshold (ImageJ) from A: backscatter electron Image 6 of Òdena quarry sample D2 (AA-3). B: Greyscale threshold settings defined to quantify %. SrOx = accessory phases. C: Image 6 with all pixels that fall into the gypsum threshold in red. See Table S1 for further results.

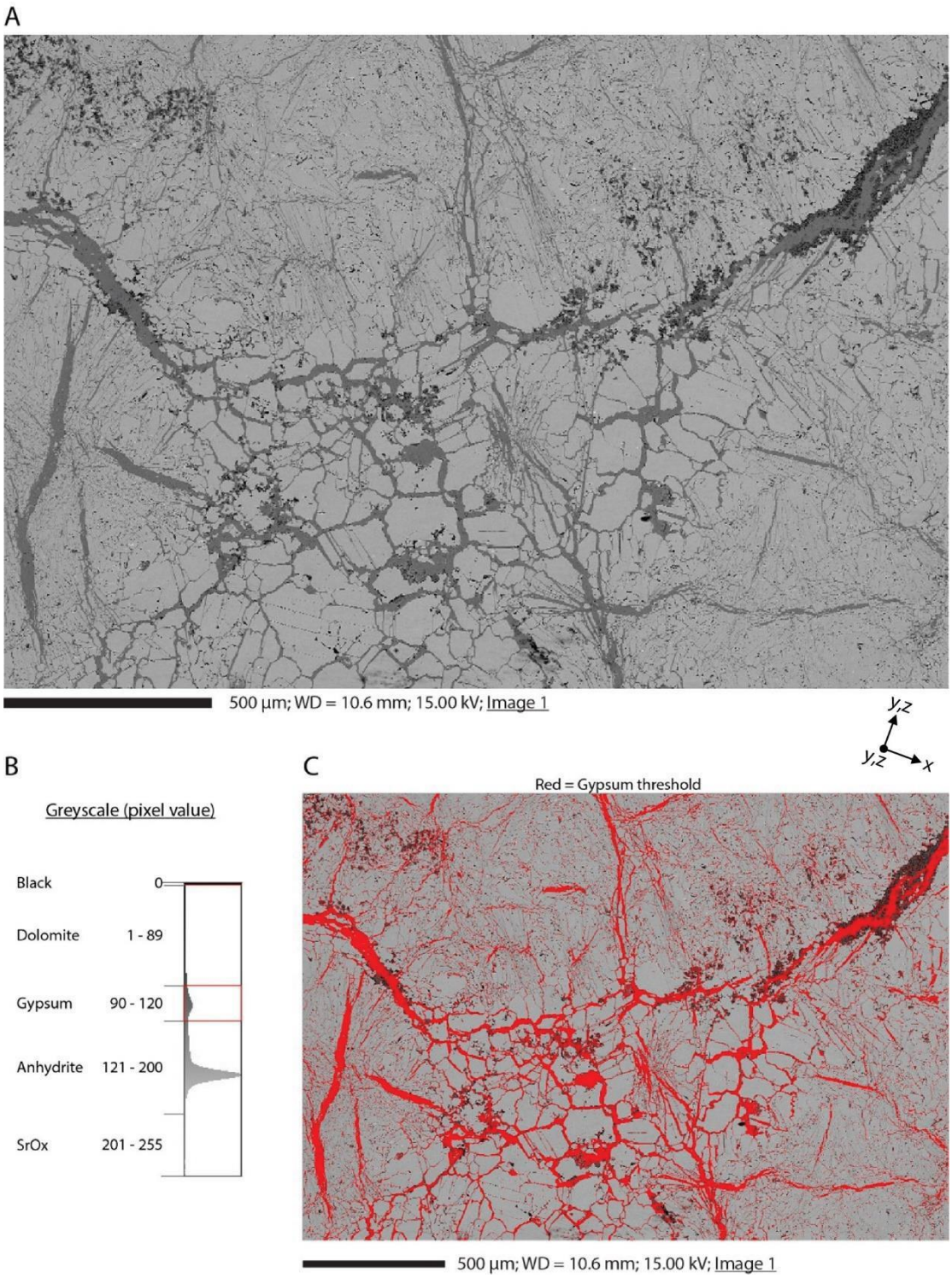

Fig. S19: Phase content analysis via greyscale threshold (ImageJ) from A: backscatter electron Image 1 of Òdena quarry sample H2 (BA-4) after constant stress differential compaction (CSDC). The section where Image 1 was taken is from a part of the sample that shows no sign of shear fractures. B: Greyscale threshold settings defined to quantify %. SrOx = accessory phases. C: Image 1 with all pixels that fall into the gypsum threshold in red. See Table S1 for further results. The location of the image is marked as 'Image 1' in Fig. S11.

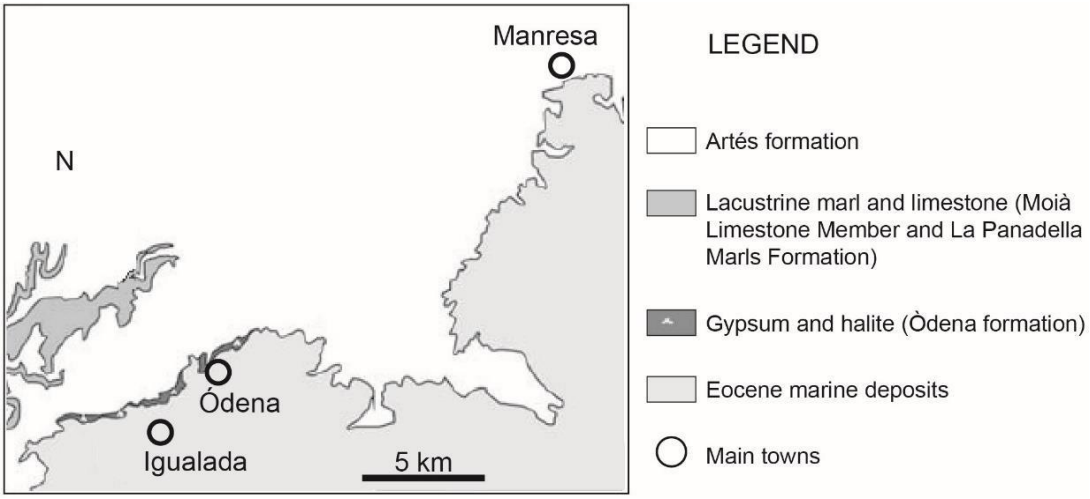

Fig. S20: Geological setting of the north eastern part of the Ebro Foreland Basin with the location of the Ódena formation (map modified from Sanjuan et al., 2014)

Sanjuan, J., Martín-Closas, C., Costa, E., Barberà, X., and Garcés, M.: Calibration of Eocene-Oligocene charophyte biozones in the Eastern Ebro Basin (Catalonia, Spain), Stratigraphy, 11, 61-81, 2014.

S2 Tables

Table S1: Phase content greyscale threshold analysis on four backscatter electron images from two Òdena quarry samples from sections with no visible impact from deformation or hydration. Image 1 is from BA-4h (H2) after constant stress differential compaction, but from a section that shows no sign of hydration through the experiment. Figures A16 to A19 present the Images and thresholds used for the analysis. Hal = halite, gyp = gypsum, dol = dolomite, SrO_x = accessory phases, black = open fractures. Deviation = difference between the image area and the sum of the pixels that were sorted by the greyscale threshold. SUM is the content calculated by adding phase area up, meaning that the different images were treated as one. Mean is the statistic mean of all four grey scale threshold case studies, and STDEV is the corresponding standard deviation. The marked values (bold) are the data used as initial material phase content for Òdena quarry anhydrite in the study.

	D2 (AA-3)			H2 (BA-4)			
	Image 2	Image 5	Image 6	Image 1	***SUM***	***Mean***	***STDEV***
Image Area [px²]	724992	724992	724992	724992	2899968		
Image Area [µm²]	724992.00	7080000.00	875482.57	2837203.17	11517677.74		
Anh Area [µm²]	616855.00	5943632.86	720518.20	2283682.42	9564688.49		
Gyp Area [µm²]	87018.00	962200.66	111973.72	403149.46	1564341.84	391085.46	406890.03
Dol Area [µm²]	20165.00	168674.00	39121.10	139005.57	366965.67	91741.42	73131.40
SrO_x Area [µm²]	96.00	175.78	227.08	5008.77	5507.63	1376.91	2421.84
Black [µm²]	858.00	5215.01	3654.93	6351.00	16078.93	4019.73	2379.99
Sum [µm²]	724992.00	7079898.32	875495.03	2837197.22	11517582.57	2879395.64	2961028.89
Deviation [µm²]	0.00	101.68	-12.46	5.96	95.17		
Deviation [%]	0.00	0.00	0.00	0.00	0.00083	0.00	0.00
Anh [%]	85.08	83.95	82.30	80.49	83.04	**82.96**	2.00
Gyp [%]	12.00	13.59	12.79	14.21	13.58	**13.15**	0.96
Dol [%]	2.78	2.38	4.47	4.90	3.19	**3.63**	1.24
SrO_x [%]	0.01	0.00	0.03	0.18	0.05	**0.05**	0.08
Black [%]	0.12	0.07	0.42	0.22	0.14	**0.21**	0.15